# Combined Microwave Radiometer and Altimeter Retrieval of Wet Path Delay for the GEOSAT Follow-On

Christopher S. Ruf, *Senior Member, IEEE,* Rajiv P. Dewan, and Bala Subramanya, *Member, IEEE*

*Abstract*— **The GEOSAT follow-on (GFO) satellite includes a two-frequency water vapor radiometer (WVR) operating at 22.2 and 37.0 GHz to correct for the path delay of its altimeter signal through the wet troposphere. Path delay retrievals based on two-frequency radiometer measurements alone include a residual bias which is correlated with either cloud liquid water or surface wind speed, depending on the choice of frequencies. The GFO WVR frequencies were chosen in part to correlate the bias with wind speed. This wind speed is then estimated and the bias corrected by using the radar cross-section data available from the altimeter. The specific algorithm by which this correction is implemented, together with estimates of its accuracy and sensitivity to measurement error, are presented. A final path delay retrieval accuracy of 1.18 cm rms is expected on orbit. This assumes absolute calibration of the WVR brightness temperatures to ±1.0 K and of the altimeter radar cross section to ±0.5 dB. The performance of a modified version of the path delay retrieval algorithm (to operate at 21 and 37 GHz) is also tested using a two frequency subset of the TOPEX/Poseidon microwave radiometer (TMR) flight data over ground calibration sites.**

## I. Introduction

THE U.S. Navy's GEOSAT follow-on (GFO) oceanography satellite is based on the earlier GEOSAT mission [1]. Both the original GEOSAT and GFO use a radar altimeter to map the ocean surface topography. Additional performance demands which were placed on the GFO mission necessitated the inclusion of an on-board water vapor radiometer (WVR) to monitor and correct for the path delay of the altimeter signal due to water vapor and cloud liquid water in the troposphere. All satellite altimeter missions have required some form of wet path delay correction, due to the highly variable spatial and temporal distribution of the water vapor [2]. The SeaSat and Nimbus 7 missions used an on-board instrument, the scanning multichannel microwave radiometer (SMMR) [3], [4]. GEOSAT did not have an on-board WVR and so used interpolated values from SMMR and from the Fleet Numerical Oceanography Center (FNOC) [5]. The ERS-1 mission uses an on-board radiometer, the along track scanning radiometer/microwave radiometer (ATSR/MWR) [6]. The TOPEX/Poseidon also uses an on-board radiometer, the TOPEX microwave radiometer (TMR) [7], [8].

The performance of the wet path delay correction for each of these missions varies. GEOSAT corrections can require a significant degree of interpolation in both space and time from the SMMR or FNOC measurements to the GEOSAT altimeter data space. RMS errors on the order of 25–30% of the total path delay (which ranges over ≈5–50 cm from polar to tropical conditions) have been reported using FNOC corrections [9] and rms errors of approximately 10% can be expected with an improved numerical grid provided by the French Meteorological Office (FMO) [10]. The correspondence between these relative errors and global rms absolute errors is determined by a weighted average over the global distribution of path delay values. Thus, rms errors of slightly larger than 25–30% and 10% of the global mean path delay of ≈17 cm can be expected for FNOC and FMO, respectively. However, errors in the FNOC and FMO models can reach 10–20 cm near small scale structures such as atmospheric fronts [3]. SMMR measurements used by the on-board altimeters of SeaSat and Nimbus 7 required only a spatial interpolation, because the radiometer and altimeter beams were not coaligned. An rms error of 2.5 cm is estimated in this case [11]. On-board radiometers which are also co-aligned with the altimeter perform the best. An rms error of 2.0 cm is estimated in the case of ERS-1, using a radiometer which operates at 23.8 and 36.5 GHz [12]. The error is reduced to an estimated 1.2 cm in the case of the TMR on-board TOPEX, which operates at 18.0, 21.0, and 37.0 GHz [13]. TMR performance has also been demonstrated in flight with 1.1 cm of rms error [14].

The last two examples cited above illustrate an important WVR design issue which is addressed in this paper. Variability in the brightness temperature (TB) measurements made by a satellite WVR is due primarily to changes in the ocean surface emissivity—due to changes in the surface wind speed—and to changes in the integrated atmospheric water vapor and cloud liquid water content. Whereas it is the integrated water vapor that affects the wet path delay, all three variables affect the WVR data. Three-frequency WVR's can separate the contributions to the TB measurements made by the three variables by identifying differences in the spectral behavior of their microwave emission. Two-frequency WVR's require the wet path delay retrieval algorithm to be "tuned" in some sense to nominal conditions in either wind speed or cloud liquid. Thus, a three-frequency WVR will perform better than

Manuscript received March 9, 1995; revised November 17, 1995. This work was supported in part by the Applied Physics Laboratory, Johns Hopkins University.

C. S. Ruf and R. P. Dewan are with the Department of Electrical Engineering, Pennsylvania State University, University Park, PA 16802 USA (e-mail: ruf@rufece.psu.edu).

B. Subramanya was with the Department of Electrical Engineering, Pennsylvania State University, University Park, PA 16802 USA. He is now with NASA Goddard Space Flight Center, Greenbelt, MD 20771 USA.

Publisher Item Identifier S 0196-2892(96)02855-0.

a two-frequency WVR but at additional costs in hardware complexity, mass, size, and power. This paper attempts to remove the additional error incurred by using a two-frequency WVR by incorporating additional information about the surface wind speed which is available from the coincident radar cross-section measurements made by the altimeter.

The performance of the wet path delay retrieval algorithm for the GFO WVR is simulated using a large data base of atmospheric profiles assembled from island launched radiosondes, together with a statistical data base of typical sea surface temperature and wind speed conditions. The data base is described in the following section. Next, the wet path delay retrieval algorithm is presented, including a wind speed bias correction which uses the altimeter radar cross-section information. The issue of frequency selection is then addressed in a comparison study between various two-frequency algorithms. The performance of the particular two-frequency choice selected for GFO, namely 22.2 and 37.0 GHz, is discussed in the remaining sections. First, the GFO algorithm is tested against an independent subset of the radiosonde data base. Next, a modified GFO algorithm, using 21.0 and 37.0 GHz, is tested on the TOPEX TMR in flight intercomparison data base and compared with the TMR three-frequency algorithm. Finally, a sensitivity analysis is presented to justify the use of 22.2, rather than 21.0, GHz as the primary water vapor channel.

## II. Atmospheric and Sea Surface Data Base

The data base of atmospheric profiles which was used in this study was assembled from 28 open ocean island sites of routine (roughly twice daily) radiosonde launches. All 28 sites lie on or very near the ground track of the TOPEX/Poseidon satellite and are well distributed in latitude and longitude over the globe. Balloon launches which coincide in time with TOPEX overpasses are used to calibrate and monitor the performance of the TMR [14]. All balloon launches from August 1992 through December 1994, totaling 29 172 launches after a number of quality screening procedures, were used in this study. The atmospheric profiles can be converted to wet path delay using the relation [15]

$$\mathrm{PD} = \int_0^\infty \left[0.001\,763\frac{\rho v(z)}{T(z)} + 0.0016L(z)\right] dz \qquad (1)$$

where PD (cm) is the wet path delay due to both water vapor and cloud liquid water, $\rho_v$ (g/m$^3$) is the absolute humidity profile, $T$ (K) is the air temperature profile, $L$ (g/m$^3$) is the cloud liquid water profile, and $z$ (m) is the altitude. The liquid profile is estimated from the measured profiles of temperature and humidity by assuming that 50% of the difference between the measured absolute humidity and the absolute humidity predicted by moist adiabatic expansion of the air inside a cloud is converted to liquid [15]. The presence of clouds is flagged by relative humidities in excess of 94%. For purposes of this study, this liquid water estimator does not need to accurately predict the actual cloud liquid water present during each individual balloon launch. Instead, it needs to generate a reasonable statistical representation of the variety of liquid profiles and the covariance of liquid profiles with those of absolute humidity and temperature.

The sea surface wind speed and water temperature below each radiosonde during launch are estimated from climatological statistics. A monthly mean sea surface temperature is designated independently for each radiosonde launch site. These statistics are derived from [16], based on the longitude and latitude of the site. The average wind speed for each launch site is also found in [16]. Specific random realizations of the surface winds are derived from these statistics by assuming a Rayleigh distribution of the wind, given the mean. Ten independent wind realizations are made for each balloon profile, effectively multiplying the size of the data base by ten and providing a reasonable statistical representation of the global wind distribution.

Satellite brightness temperature measurements are simulated by inserting the atmospheric profiles and surface conditions described above into the appropriate equation of radiative transfer

$$\mathrm{TB}(f) = T_{\mathrm{up}} + [(T_{\mathrm{dn}} + T_c e^{-\tau})(1-\varepsilon) + \varepsilon T_s]e^{-\tau} \qquad (2)$$

where TB (K) is the measured brightness temperature at the satellite, $T_{\mathrm{up}}$ and $T_{\mathrm{dn}}$ (K) are the upwelling and downwelling brightness from the atmosphere, respectively, $T_c$ (K) is the cosmic background brightness, $\varepsilon$ is the surface emissivity, $T_s$ (K) is the physical temperature of the sea surface, and $\tau(N_p)$ is the opacity of the atmosphere. Explicit expressions for each of the terms in (2) are given in the literature (e.g., [13], [17]). It should be noted that the dependence of atmospheric absorption on frequency, temperature, pressure, and water vapor used in this study is based on refinements to the models of Liebe and Layton [18] and Liebe, Rosenkranz, and Hufford [19], as discussed in [14] and [20]. These are small ($\approx$5%) corrections to the 22.235 GHz water vapor line strength and water vapor and oxygen continuum absorption which are based on recent ground and satellite based intercomparisons with radiosonde profiles.

A summary of the data base assembled for this study is given in Table I. Humidity, cloud, wind speed, and sea surface temperature statistics for each launch site are listed, together with the number of atmospheric profiles available at each site after screening for data quality.

## III. Wet Path Delay Algorithm

The GFO WVR wet path delay retrieval algorithm is a modification of the three-frequency algorithm used by the TMR [13] which uses only two-frequencies but includes the altimeter radar cross section as an additional source of information. The decision to use two WVR frequencies, rather than the three frequencies used by TMR, was based on size, power, antenna complexity, and, ultimately, cost constraints on the GFO mission. The two-frequency algorithm can be expressed to first order as a linear combination of the WVR brightness temperatures

$$\mathrm{PD} = c_{0,\,\mathrm{global}} + c_{1,\,\mathrm{global}}\mathrm{TB}ff_1 + c_{2,\,\mathrm{global}}\mathrm{TB}ff_2 \qquad (3)$$

where PD is the wet path delay and $\mathrm{TB}ff_i$ is the brightness temperature at frequency $ff_i$. The retrieval coefficients

TABLE I
SUMMARY OF GLOBAL DATA BASE OF ATMOSPHERIC AND SEA SURFACE CONDITIONS USED TO TRAIN AND TEST THE GFO WVR WET PATH DELAY RETRIEVAL ALGORITHM

| Station ID Number | Lat deg North | Lon deg East | Total points | Mean PD (cm) | Stddev PD (cm) | % clear | % cloudy | Mean liq in clouds (microns) | Mean SST (°C) | Mean wind speed (m/s) |
|---|---|---|---|---|---|---|---|---|---|---|
| 72393 | 34.75 | -121 | 1346 | 12.01 | 3.57 | 86 | 14.12 | 193 | 16 | 8.84 |
| 16429 | 37.92 | 12.5 | 2276 | 11.7 | 3.63 | 98 | 1.89 | 246 | 14.1 | 9.62 |
| 43333 | 11.67 | 92.72 | 577 | 24.96 | 6.8 | 95 | 4.68 | 464 | 29.8 | 11.99 |
| 43369 | 8.3 | 73 | 699 | 22.64 | 26.32 | 93 | 7.44 | 359 | 31.9 | 7.80 |
| 47678 | 33.1 | 139.8 | 1604 | 16.84 | 7.17 | 96 | 4.24 | 215 | 17 | 6.80 |
| 47909 | 28.38 | 129.5 | 1613 | 17.24 | 6.41 | 97 | 3.16 | 267 | 19.8 | 12.73 |
| 47936 | 26.23 | 127.7 | 2009 | 21.39 | 6.79 | 97 | 2.89 | 290 | 21.1 | 8.35 |
| 47945 | 25.83 | 131.2 | 2138 | 22.31 | 5.23 | 98 | 2.39 | 315 | 21.3 | 8.98 |
| 47971 | 27.08 | 142.2 | 1849 | 21.57 | 6.16 | 97 | 3.3 | 238 | 20.6 | 7.14 |
| 61902 | -7.97 | -14.4 | 248 | 17.61 | 3.94 | 48 | 52.42 | 327 | 27.7 | 7.09 |
| 61967 | -7.3 | 74.48 | 91 | 9.98 | 17.66 | 91 | 8.79 | 306 | 27.9 | 6.24 |
| 68906 | -40.4 | -9.88 | 70 | 8.63 | 3.27 | 90 | 10 | 489 | 14.7 | 6.38 |
| 68994 | -46.9 | 37.87 | 59 | 725 | 4.2 | 97 | 3.39 | 657 | 12.1 | 7.80 |
| 70308 | 57.15 | -170 | 1456 | 9.05 | 2.67 | 46 | 53.64 | 268 | 2.6 | 12.41 |
| 71600 | 43.93 | -60 | 1024 | 11.16 | 3.24 | 69 | 30.76 | 250 | 10.5 | 10.38 |
| 78016 | 32.37 | -64.7 | 181 | 16.34 | 6.28 | 85 | 14.92 | 229 | 17.4 | 8.99 |
| 78866 | 18.05 | -63.1 | 388 | 18.12 | 9.67 | 68 | 31.96 | 283 | 26 | 7.27 |
| 78954 | 13.07 | -59.5 | 762 | 22.13 | 4.73 | 73 | 27.3 | 303 | 29 | 13.67 |
| 80001 | 12.58 | -81.7 | 181 | 24.83 | 7.49 | 54 | 46.41 | 341 | 29.3 | 8.56 |
| 91217 | 13.55 | 144.8 | 1148 | 24.64 | 23.48 | 54 | 46.17 | 348 | 28.7 | 10.44 |
| 91245 | 19.28 | 166.7 | 1356 | 22.96 | 4.93 | 67 | 32.74 | 326 | 25.3 | 7.90 |
| 91348 | 6.97 | 158.2 | 820 | 28.53 | 4.91 | 54 | 46.1 | 404 | 32.7 | 9.80 |
| 91643 | -8.52 | 179.2 | 757 | 24.55 | 17.64 | 94 | 6.08 | 237 | 27.4 | 6.95 |
| 94299 | -16.3 | 150 | 1110 | 15.55 | 4.52 | 98 | 2.25 | 355 | 24.3 | 8.32 |
| 94996 | -29.1 | 167.9 | 1045 | 10.93 | 3.09 | 98 | 1.72 | 213 | 19.2 | 7.67 |
| 91413 | 9.48 | 138.1 | 787 | 27.58 | 6.08 | 47 | 52.6 | 274 | 31.2 | 9.48 |
| 96996 | -12.2 | 96.83 | 1527 | 19.49 | 5.22 | 83 | 16.9 | 275 | 26.1 | 8.86 |
| Global | - | - | 29172 | 18.8 | 10.12 | 85 | 15.43 | 297 | - | - |

$c_0 - c_2$ are found by minimum squared error regression analysis using the simulated data base. This is a statistical inversion approach, and has been applied to many similar atmospheric inversion problems (e.g., [21], [22]). Due to second order nonlinearities in the relationship between PD and TB, the residual error in this regression fit is improved by stratifying the data base into subsets of the path delay and the cloud liquid water content. The cloud liquid water content, LIQ, is also estimated by a linear combination of TB's:

$$\mathrm{LIQ} = c_{0,\,\mathrm{liquid}} + c_{1,\,\mathrm{liquid}}\mathrm{TB22} + c_{2,\,\mathrm{liquid}}\mathrm{TB37} \quad (4)$$

where the retrieval coefficients $c_0 - c_2$ are also found by regression analysis. The retrieval coefficients in (3) can then be expanded into subgroups appropriate for different ranges of the path delay and liquid. The stratified wet path delay retrieval algorithm then becomes

$$\mathrm{PD}_2 = c_{0,\mathrm{PD,LIQ}} + c_{1,\mathrm{PD,LIQ}}\mathrm{TB22} + c_{2,\mathrm{PD,LIQ}}\mathrm{TB37} \quad (5)$$

where PD is a first guess at the path delay (made by using (3) with coefficients $c_0 - c_2$ derived from a global distribution of path delays), LIQ is the liquid water estimate made using (4), and the coefficients $c_{i,j,k}$ are derived from appropriate subsets

of distributions of the path delay and liquid water content. The residual error in this stratified regression fit can be further improved slightly, and the dependence of the bias in the fit on ocean surface wind speed can be reduced significantly, by removing the wind speed dependent bias

$$\mathrm{PD}_3 = \mathrm{PD}_2 + \delta\mathrm{PD}(\mathrm{WS}) \tag{6}$$

where $\delta$PD is a tabulated list of PD bias corrections versus wind speed, WS. The bias correction at each wind speed level is determined by the average difference between the true path delay, as defined by the radiosonde profiles, and the path delay retrieved using (5). The wind speed is determined from $\sigma_o$, the normalized radar cross section measured by the radar altimeter.

The need in two-frequency algorithms for a bias correction such as that described by (6) has been noted by Keihm *et al.*, [13]. They considered the issue from the perspective of evaluating the expected performance of the TMR, should one of its nonredundant channels fail. (The 18 and 37 GHz channels are nonredundant, while the 21 GHz channel has a back up.) It was noted that a failure of the 18 GHz channel would produce a wind speed dependent bias in the wet path delay retrieval, whereas a failure of the 37 GHz channel would produce a cloud liquid water dependent bias. This behavior can be readily explained by considering the spectral behavior of the cloud liquid water and wind speed induced brightness. The liquid water brightness has a strong ($\propto f^2$)-frequency dependence [23] and the wind speed induced excess emissivity of the ocean surface is essentially independent of frequency over the range of frequencies that are of interest here [24]. Thus, widely spaced frequencies (such as 21 and 37 GHz in the case of TMR) can more easily identify the liquid water effect on the measured brightness. Closely spaced frequencies (such as 18 and 21 GHz), on the other hand, are much more sensitive to measurement noise when trying to separate the liquid component of the brightness. Recall that these retrieval algorithms use statistical inversion with measurement noise added to the simulated data base. The regression analysis determines retrieval coefficients which explain the largest possible fraction of the variance in the path delay. In the case of the 18 and 21 GHz algorithm, the noise in the simulated data tends to mask the small cloud signature in the data. The regression fit cannot identify the component of the variance in the brightness due to liquid water, so it effectively tunes the retrieval to the average cloud conditions in the data base. This results in a liquid dependent bias in the path delay estimates. In the 21 and 37 GHz case, the same level of additive noise will not mask the cloud signature as much, since there is a larger difference in their responses to liquid. The variance in the brightness due to liquid water is largely explained by the regression fit, leaving the retrieval tuned to the average wind speed in the data base.

The retrieval coefficients derived for GFO are listed in Tables II and III. These tables include coefficients for the global retrieval of wet path delay and cloud liquid, the stratified retrieval of wet path delay, and the wind speed dependent wet path delay bias correction. As noted above, this retrieval is an optimal estimator in the sense that *a priori* information about the climatological mean and variability of the wet path delay has been weighted against the error in the retrieval due to measurement noise in the brightness temperatures. This is incorporated into the minimum-squared-error regression analysis by adding typical levels of noise (1.0-K rms) to the simulated brightness temperatures before regressing against the wet path delay.

TABLE II
GFO WVR WET PATH DELAY RETRIEVAL ALGORITHM COEFFICIENTS

| Bin | $C_0$ | $C_1$ | $C_2$ |
|---|---|---|---|
| Global PD | -43.513 | 0.422 | -0.090 |
| Global Liq | -2271.387 | -5.980 | 20.831 |
| 0≤PD<10; LIQ<100 | -25.939 | 0.281 | -0.059 |
| 10≤PD<20; LIQ<100 | -53.544 | 0.321 | 0.082 |
| 20≤PD<30;LIQ<100 | -63.882 | 0.381 | 0.081 |
| 30≤PD; LIQ<100 | -49.351 | 0.226 | 0.193 |
| 0≤PD<10; LIQ≥100 | -12.147 | 0.246 | -0.111 |
| 10≤PD<20; LIQ≥100 | -32.252 | 0.413 | -0.151 |
| 20≤PD<30; LIQ≥100 | -47.306 | 0.474 | -0.128 |
| 30≤PD; LIQ≥100 | -43.773 | 0.443 | -0.106 |

TABLE III
WIND SPEED DEPENDENT WET PATH DELAY RETRIEVAL BIAS CORRECTIONS

| Bin (m/s) | 0 - 7 | 7 - 10 | 10 - 13 | 13 -16 | 16 - 19 | 19 - 22 | > 22 |
|---|---|---|---|---|---|---|---|
| Bias (cm) | 0.22850 | 0.03592 | -0.38714 | -0.81554 | -1.18394 | -1.35222 | -2.07217 |

The estimation of wind speed from the radar altimeter is based on the tabulated values provided by the modified Chelton-Wentz (MCW) algorithm [25]. MCW provides a mapping from radar cross section, $\sigma_o$, to wind speed referenced to 19.5 m above the ocean surface. This mapping extends over the range 19.6–7.0 dB and 0–20.2 m/s for $\sigma_o$ and wind speed, respectively, and has an estimated accuracy of 2 m/s rms. Higher wind speeds, corresponding to radar cross sections below 7.0 dB, are estimated by linear extrapolation of the last two entries in the look up table. Radar cross sections above 19.6 dB are all assumed to correspond to 0 m/s wind speed. Such high values for $\sigma_o$ would generally be due to the additive noise present in the radar system. The effect that this has on the path delay bias correction is negligible because the wind induced excess emissivity of the ocean surface at these microwave frequencies becomes significant only above $\approx$7 m/s [24].

## IV. TWO FREQUENCY ALGORITHM COMPARISON

The selection of WVR frequencies can be addressed by considering the performance of a class of two-frequency algorithms. A class of global, nonstratified wet path delay retrieval algorithms was tested in which one frequency was fixed at 22.2 GHz and the other was varied from 18 to 37 GHz. This bilinear algorithm is described by (3). The rms residual error in each algorithm was evaluated by deriving the bilinear regression coefficients using 50% of a global data base of atmospheric and surface conditions and testing against the other 50%. 1.0-K rms noise was added to brightness temperatures in both halves of the data base. This adds an optimal estimation weighting to the retrieval coefficients

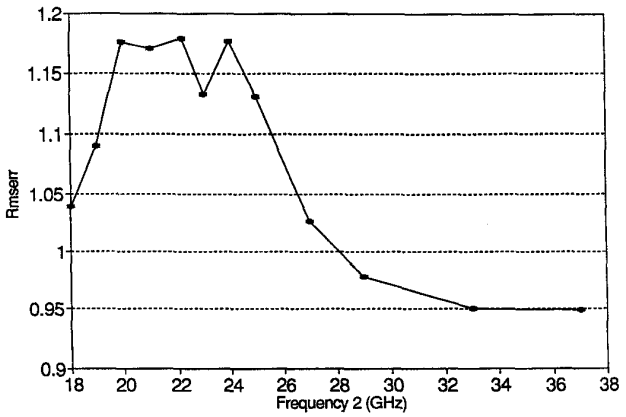


Fig. 1. Two-frequency wet path delay retrieval performance as a function of the second frequency, assuming the first frequency is 22.2 GHz. Closely spaced pairs of frequencies have difficulty resolving the spectral differences between water vapor and cloud liquid water effects on the brightness temperature in the presence of measurement noise. The GEOSAT follow-on water vapor radiometer (GFO WVR) will operate at 22.2 and 37.0 GHz.

with respect to climatology, and it includes the effects of sensitivity by the algorithms to measurement noise in the residual errors. The results are shown in Fig. 1. Note from the figure that the behavior of the residual error with respect to the second frequency is approximately symmetric about the first frequency. Second frequencies very near the first frequency contribute little additional information and so the RSS error is higher. Second frequencies farther from the first have lower RSS errors, with the 37 GHz second frequency performing best since it is better able to resolve the liquid water component of the brightness temperature.

The decision by GFO to use 37 GHz as the second frequency was based in part on this performance analysis, in part on the desire to force a correlation of the residual wet path delay error with wind speed, which can be indirectly measured by the altimeter, rather than with cloud liquid, which can not, and in part on the desire to operate with a frequency similar to TMR so that its heritage can be utilized as much as possible. The decision to use 22.2 GHz as the first frequency, rather than 21 GHz as in TMR, was based primarily on sensitivity considerations which are discussed below.

## V. GFO Wet Path Delay Algorithm Performance

### A. Radiosonde Data Base Test

The regression coefficients in the GFO wet path delay retrieval algorithm are derived from a random selection of 50% of the global data base described above. The retrieval performance was then tested against the other 50%. The data base consists of simulated TB's and their corresponding wet path delays and surface wind speeds. In order to simulate the performance of the radar altimeter, the wind speeds were converted to $\sigma_o$ according to the MCW relation. The performance of the algorithm was tested in the presence of measurement error by adding uncorrelated zero mean Gaussian noise to both the simulated TB's and $\sigma_o$ prior to inversion. In the case of the wind speed bias correction, the inversion of $\sigma_o$ amounts simply to a reverse application of the MCW relation. The rms difference between the GFO retrieved and the actual wet path delays for the case of no measurement error is 0.64 cm. This compares favorably to the comparable three-frequency TMR residual error level of 0.37 cm [13], and represents a measure of the information lost in going from a three to a two-frequency radiometer. If TB noise of 1.0-K rms and $\sigma_o$ noise of 0.5 dB rms are added to the simulated data, the residual error increases to 0.77 cm.

Several scatter plots of the error in the wet path delay retrieval ($PD_{true} - PD_{retrieved}$) demonstrate its performance. These plots are all for the case of 1.0 K and 0.5 dB rms measurement noise in TB and $\sigma_o$, respectively. For clarity in the presentation, they show a random sampling of 1900 out of the 72 930 retrievals on which the rms error levels quoted above are based. Fig. 2 shows the wet path delay error versus surface wind speed before the altimeter wind speed bias correction has been applied. Note that the two-frequency algorithm increasingly over estimates the wet path delay as the wind speed increases. This is consistent with the results presented by Keihm *et al.* [13] using a 21.0 and 37.0 GHz algorithm. The bias is not significant with respect to the other intrinsic scatter in the retrieval process at wind speeds below $\approx$10 m/s. Since the global wind speed distribution is fairly tightly concentrated at these lower values, the bias has little effect on the overall rms error in the retrieval. However, regions with statistically high winds will be consistently biased. Fig. 3 shows the error in the full wet path delay retrieval algorithm, including an altimeter derived wind speed bias correction, versus wet path delay, integrated cloud liquid water content, and surface wind speed. In each case, note that the scatter is not significantly greater in any particular range of the free parameter (the abscissa), and that there is no significant correlation between the error and the free parameter. The correlation with wet path delay has been removed by the stratification scheme, the correlation with cloud liquid has been removed by the use of two widely separated frequencies, and the correlation with wind speed has been corrected by use of the altimeter radar cross-section measurements.

### B. TOPEX Intercomparison Test

The radiosonde data base test described above is internally consistent, in that the wet path delay retrieval algorithm was trained using half of the data base and tested using the other half. Many types of errors in the generation of the data base could easily go undetected by this procedure. They could result in a retrieval algorithm with a low rms residual error, according to the test described above, but with a significantly larger actual error in practice. An independent test of the retrieval algorithm and, indirectly, of the integrity of the data base was conducted by deriving new algorithms at 21 and 37 GHz and at 18, 21, and 37 GHz from the data base and then testing them using TMR in flight intercomparison data. The two-frequency algorithm at 21 and 37 GHz is identical in form to the 22.2 and 37 GHz GFO algorithm described above. (A sensitivity comparison between these two algorithms is the subject of the following section.) The three-frequency

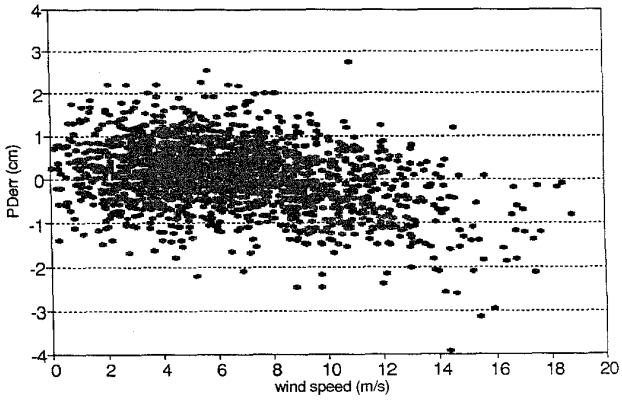


Fig. 2. Error in GFO 22.2 and 37.0 GHz wet path delay retrieval versus ocean surface wind speed without a bias correction for the wind speed. The path delay is increasingly over estimated as the wind speed increases. A correction can be made using the coincident radar altimeter measurements of radar cross section.

algorithm derived here, at 18, 21, and 37 GHz, is similar to the official TMR algorithm used for TOPEX Project data processing (hereafter referred to as official TMR) [13]. It does not include a wind speed correction but does stratify the retrieval with respect to both wet path delay and cloud liquid water content. (The official TMR algorithm also stratifies with respect to wind speed, for a small additional improvement in retrieval performance.)

The intercomparison data consist of 1009 overpasses by TMR of open ocean island radiosonde launch sites within 150 km of the satellite ground track and within 150 minutes of a balloon launch. The data were compiled during the period September 1992 through October 1995, and are an updated version of the data described by Ruf *et al.* [14]. Each overpass provides direct radiosonde measurement of the wet path delay together with direct TMR measurements of TB at 18, 21, and 37 GHz. In addition, the official TMR algorithm also retrieves surface wind speed from the three-frequency TB measurements. This value is converted to $\sigma_o$ using the MCW relation and is used as input to the two-frequency, 21-and-37-GHz algorithm.

The rms difference between the radiosonde determined (true) wet path delay and each of the retrieved path delays was determined. The values are 2.26 cm for the official TMR wet path delay, 2.30 cm for the three-frequency algorithm derived here, and 2.78 cm for the two-frequency algorithm at 21 and 37 GHz. The slightly better three-frequency performance by the official TMR algorithm can be explained by the more elaborate stratification they use with respect to wind speed in addition to wet path delay and cloud liquid. Fig. 4(a)–(c) show scatter plots comparing the two- and three-frequency retrievals. The retrieved wet path delay is plotted versus the "true" value as determined by the radiosonde. There are numerous sources of spatial and temporal decorrelation error and of error in the radiosonde data itself which accounts for most of the rms difference between these wet path delay estimates [14]. While the scatter is slightly greater for the two-frequency retrieval, there is no significant bias or wet path delay dependent error in the two-frequency retrieval.

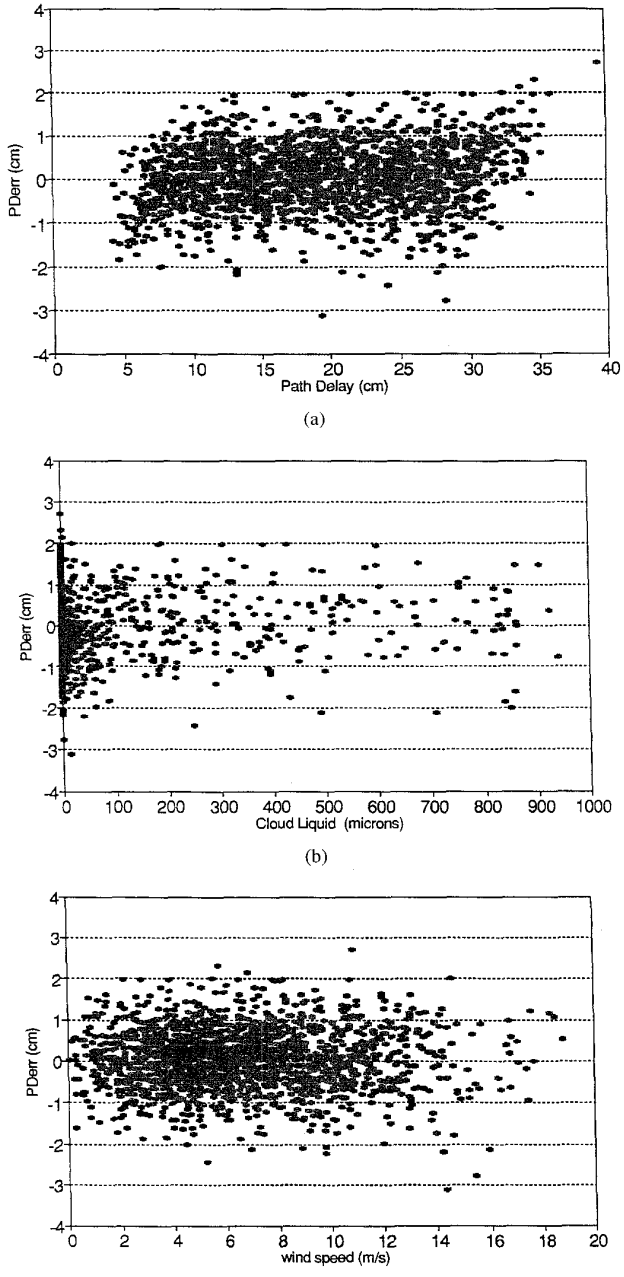


Fig. 3. Error in GFO 22.2 and 37.0 GHz wet path delay retrieval with altimeter derived bias correction included, versus: (a) true path delay, (b) cloud liquid water content, and (c) ocean surface wind speed. These scatter plots assume 1.0-K and 0.5-dB rms zero mean noise in the simulated brightness temperature and radar cross-section data, respectively.

It should be noted that, while this intercomparison test validates most aspects of the data base from which the path delay algorithm is derived, it assumes that the MCW relationship between $\sigma_o$ and wind speed is exact. Specifically, wind speeds measured by TMR are converted to $\sigma_o$ using MCW. These values of $\sigma_o$ are used as input to the path delay algorithm, as if they were actually measured by the altimeter.

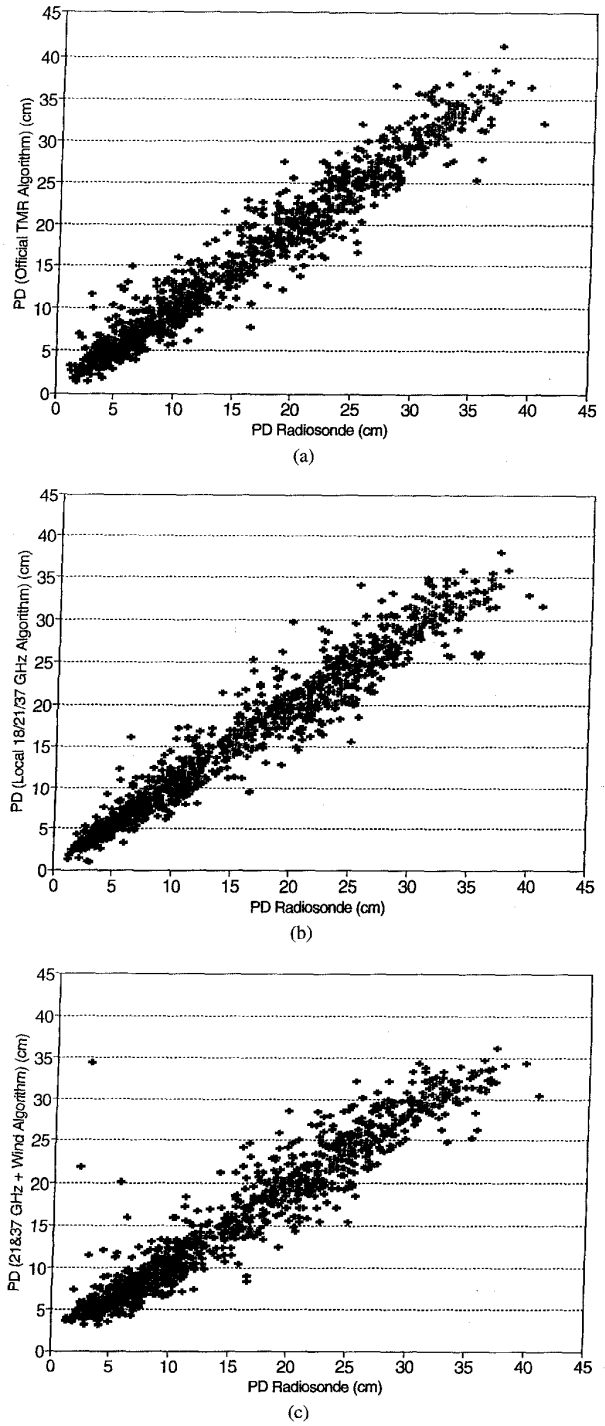


Fig. 4. Radiosonde derived "true" wet path delay versus path delay estimated from the TOPEX microwave radiometer (TMR) intercomparison data base accumulated during September 1992 through July 1994. Each data point represents one of 1009 TOPEX satellite overpasses of an island site within 150 km and 150 min of a radiosonde launch. For clarity, 9 outlier points with retrieval errors of $\geq$10 cm have been removed. Three radiometer derived estimates of path delay are shown: (a) official three-frequency TMR retrieval at 18, 21, and 37 GHz, with an rms difference from the radiosonde of 2.26 cm, (b) similar three-frequency retrieval derived from the global data base described in the text, with an rms error of 2.30 cm, and (c) GFO WVR-like 21- and 37-GHz retrieval derived from the same global data base, with an rms error of 2.78 cm.

Thus, errors in MCW, which are estimated at 2.0 m/s rms [25], have not been incorporated. However, an altimeter error of 0.5 dB rms has been included in the error analyses discussed above (see radiosonde data base test) and below (see error budget for wet path delay retrieval). This corresponds to a 2–3 m/s rms error in wind speed over the range of most common wind speeds.

### C. Sensitivity Analysis

The relative merits of a two-frequency wet path delay retrieval algorithm using 21 and 37 GHz versus 22.2 and 37 GHz are best judged in terms of the sensitivity of the two algorithms to measurement error. To this end, a number of simulations were run in which the rms error in the wet path delay retrieval was evaluated with variable levels of noise in the measured data. These simulations all used the algorithms discussed above, which were derived from a random 50% sample of the large radiosonde data base. The rms error was determined from the other 50% of the data base. Independent zero mean Gaussian noise was added to the TB's before inversion. A first order estimate of the response of these algorithms to noise is possible by simply considering the root-sum-square of TB coefficients in the global retrieval algorithm given by (3). The numerical simulation was used instead because the exact behavior of the noise sensitivity is somewhat complicated by the nonlinear character of the stratification method.

Results of the simulation are shown in Fig. 5. The 22.2/37 GHz algorithm is seen to perform better than the 21/37 GHz algorithm at all levels of noise. Most significantly, the degradation in performance of the 22.2/37 GHz algorithm with measurement noise is much more gradual. This is simply explained by the higher sensitivity of TB to changes in water vapor at the 22.235 GHz absorption line center. The superior performance of the 22.2/37 GHz algorithm with no measurement noise is a result of the statistical inversion procedure used to derive the retrieval coefficients. 1.0-K rms noise is added to the TB values which are used in the regression analysis in order that the regression fit can appropriately weight the explained variance using the TB data against the climatological variations in the wet path delay. Thus, the "zero noise" case in Fig. 5 still includes the effects of noise in the initial regression fit. Under truly zero noise conditions, the performance of the 21/37 GHz algorithm should be better than that at 22.2/37 GHz. This is suggested by the broader, less altitude dependent form of the water vapor weighting function at 21 GHz [26]. However, these results suggest that this improvement can only be realized given noise levels which are not generally attained in low Earth orbit.

## VI. Error Budget for Wet Path Delay Retrieval

The study presented above provides an estimate of the wet path delay retrieval performance of the GFO WVR assuming various levels of noise in the measured brightness temperatures and assuming 0.5-dB rms noise in the altimeter

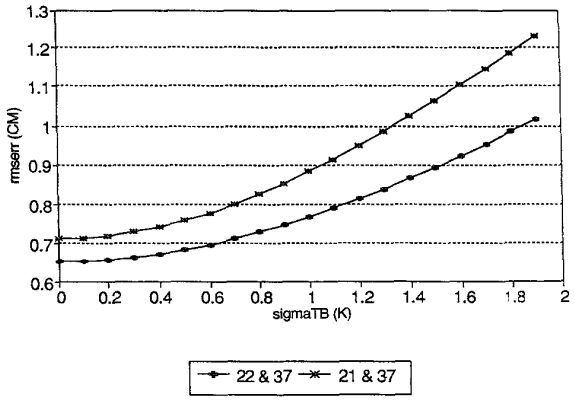


Fig. 5. RMS Error in 21/37 and 22.2/37 GHz wet path delay retrieval algorithms for varying levels of measurement noise. RMS error grows more slowly with measurement noise in the 22.2/37 GHz case. The 22.2 GHz brightness temperature is more sensitive to changes in water vapor than is 21 GHz. This reduces the effects of measurement error on the wet path delay retrieval.

measurement of ocean surface radar cross section. The level of calibration accuracy and noise in the WVR TB's is still under investigation. Based on antenna design and thermal control considerations, it is expected to be as good as or better than the ±1.1-K accuracy demonstrated by TMR [14]. As discussed above, this level of calibration would result in a wet path delay retrieval performance of 0.77 cm rms. Several additional sources of error need to be included in a comprehensive budget for the WVR performance on orbit. Uncertainties in the models used to simulate TB's from radiosonde profiles (specifically, errors in the water vapor, oxygen, and liquid water absorption, and in the specular and wind speed dependent emission by the ocean surface) are estimated by Keihm *et al.* [13] to contribute an additional 0.85 cm of error to the wet path delay retrieval. In addition, decorrelation effects due to differences in the antenna footprint sizes of the WVR and the altimeter contribute 0.25 cm of error [8]. The total (root-sum-square) expected error in the WVR is, then, 1.18 cm.

## ACKNOWLEDGMENT

The authors would like to gratefully acknowledge the use of TOPEX microwave radiometer data provided by the Jet Propulsion Laboratory (JPL), California Institute of Technology. JPL is under contract to the National Aeronautics and Space Administration.

## REFERENCES

[1] R. Barry, J. Finkelstein, C. Kilgus, C. N. K. Mooers, B. Needham, and M Crawford, "GEOSAT follow-on satellite to supply ocean sciences data," *EOS, Trans., AGU*, vol. 76, no. 4, pp. 23–26, Jan. 1995.

[2] J. Saastamoinen, "Atmospheric correction for the troposphere and stratosphere in radio ranging of satellites," *The Use of Artificial Satellites for Geodesy, Geophys. Monogr.*, vol. 15, pp. 247–251, 1972.

[3] B. D. Tapley, J. B. Lundberg, and G. H. Born, "The SeaSat altimeter wet tropospheric range correction," *J. Geophys. Res.*, vol. 87, no. C5, pp. 3213–3220, 1982.

[4] D. Prabhakara, H. D. Chang, and A. T. C. Chang, "Remote sensing of precipitable water over the oceans from Nimbus 7 microwave measurements," *J. Appl. Meteorol.*, vol. 21, pp. 59–68, 1982.

[5] R. E. Cheney, B. C. Douglas, R. W. Agreen, L. Miller, D. L. Porter, and N. S. Doyle, *GEOSAT Altimeter Geophysical Data User Handbook*, Nat. Ocean. Serv., Rockville, MD, NOAA Tech. Memo. NGS-46, p. 29, 1987.

[6] R. Bernard, A. Le Cornec, L. Eymard, and L. Tabary, "The microwave radiometer aboard ERS-1: Part 1—Characteristics and performance," *IEEE Trans. Geosci. Remote Sensing*, vol. 31, no. 6, pp. 1186–1198, 1993.

[7] C. S. Ruf, M. A. Janssen, and S. J. Keihm, "TOPEX/POSEIDON microwave radiometer (TMR): I. instrument description and antenna temperature calibration," *IEEE Trans. Geosci. Remote Sensing*, vol. 33, pp. 125–137, Jan. 1995.

[8] M. A. Janssen, C. S. Ruf, and S. J. Keihm, "TOPEX/POSEIDON microwave radiometer (TMR): II. Antenna pattern correction and brightness temperature algorithm," *IEEE Trans. Geosci. Remote Sensing*, vol. 33, pp. 138–146, Jan. 1995.

[9] G. H. Born, J. Wilkinson, and D. Lame, Eds., *SEASAT Gulf of Alaska Workshop Report*, Jet Propulsion Lab., Pasadena, CA, JPL Int. Doc. D622-101, vol. 1, 1979.

[10] D. Jourdan, C. Boissier, A. Braun, and J. F. Minster, "Influence of wet tropospheric correction on mesoscale dynamic topography as derived from satellite altimetry," *J. Geophys. Res.*, vol. 95, no. C10, pp. 17 993–18 004, 1990.

[11] D. Prabhakara, H. D. Chang, and A. T. C. Chang, "Remote sensing of precipitable water over the oceans from Nimbus 7 microwave measurements," *J. Appl. Meteorol.*, vol. 21, pp. 59–68, 1982.

[12] ERS-DC Project Office, *Along Track Scanning Radiometer and Microwave Sounder*, Farnborough, Hants, U.K., Ref. DC-HO-PST-SY-008, 1987.

[13] S. J. Keihm, M. A. Janssen, and C. S. Ruf, "TOPEX/POSEIDON microwave radiometer (TMR): III. Wet tropospheric range correction and pre-launch error budget," *IEEE Trans. Geosci. Remote Sensing*, vol. 33, pp. 147–161, Jan. 1995.

[14] C. S. Ruf, S. J. Keihm, B. Subramanya, and M. A. Janssen, "TOPEX/POSEIDON microwave radiometer performance and in-flight calibration," *J. Geophys. Res.*, vol. 99, no. C12, pp. 24 915–24 926, 1994.

[15] M. S. Malkevich, V. S. Kosolapov, and V. I. Statskiy, "Statistical characteristics of the vertical water content structure of cumulus clouds," *Izvestiya, Atmos. Ocean. Phys.*, vol. 17, pp. 203–210, 1981.

[16] D. Halpern, V. Zlotnicki, J. Newman, D. Dixon, O. Brown, and F. Wentz, "An Atlas of Monthly Mean Distributions of GEOSAT Sea Surface Height, SSM/I Surface Wind Speed, AVHRR/2 Sea Surface Temperature, and ECMWF Surface Wind Components During 1987," Jet Propulsion Lab., Pasadena, CA, JPL Publ. 92-3, 1992.

[17] F. T. Ulaby, R. K. Moore, and A. K. Fung, *Microwave Remote Sensing, Active and Passive*, vol. I. Reading, MA: Addison-Wesley, 1981, ch. 4.

[18] H. J. Liebe and D. H. Layton, "Millimeter wave properties of the atmosphere: Laboratory studies and propagation modeling," Nat. Telecom. Inform. Admin., Boulder, CO, NTIA Rep. 87-24, 1987.

[19] H. J. Liebe, P. W. Rosenkranz, and G. A. Hufford, "Atmospheric 60 GHz oxygen spectrum: New laboratory measurements and line parameters," *J. Quant. Spectrosc. Radiat. Transfer*, vol. 48, pp. 629–643, 1992.

[20] S. J. Keihm, "Atmospheric absorption from 20–32 GHz: Radiometric constraints on the vapor and oxygen components," in *Proc. Specialist Meeting on Microwave Radiometry and Remote Sensing Applications*, Boulder, CO, 1992, pp. 211–218.

[21] E. R. Westwater and M. T. Decker, "Application of statistical inversion to ground-based microwave remote sensing of temperature and water vapor profiles," in *Inversion Methods in Atmospheric Remote Sounding*, A. Deepak, Ed. New York: Academic, 1977, pp. 395–428.

[22] F. T. Ulaby, R. K. Moore, and A. K. Fung, *Microwave Remote Sensing, Active and Passive*, vol. III. Norwood, MA: Artech House, 1986, pp. 1295–1297.

[23] A. Benoit, "Signal attenuation due to neutral oxygen and water vapor, rain, and clouds," *Microwave J.*, vol. 11, pp. 73–80, 1968.

[24] T. T. Wilheit, "A model for the microwave emissivity of the ocean's surface as a function of windspeed," *IEEE Trans. Geosci. Electron.*, vol. GE-17, pp. 244–249, 1979.

[25] D. L. Witter and D. B. Chelton, "A GEOSAT altimeter wind speed algorithm and a model for altimeter wind speed algorithm development," *J. Geophys. Res.*, vol. 96, pp. 8853–8860, 1991.

[26] J. I. H. Askne and B. G. Skoog, "Atmospheric water-vapor profiling by ground-based radiometry at 22 and 183 GHz," *IEEE Trans. Geosci. Remote Sensing*, vol. GRS-21, pp. 320–323, 1983.

**Christopher S. Ruf** (S'85–M'87–SM'92) received the B.A. degree in physics from Reed College, Portland OR, in 1982 and the Ph.D. degree in electrical and computer engineering from the University of Massachusetts at Amherst in 1987.

He worked as a Research Assistant from 1983 to 1987 and continued during 1987–1988 as a Visiting Professor and Research Engineer, all with the Microwave Remote Sensing Laboratory at UMass. His research involved microwave radiometer instrumentation and data inversion in atmospheric and surface applications. He then joined the technical staff at NASA's Jet Propulsion Laboratory in 1988. While at JPL, his work involved the TOPEX microwave radiometer and ground-based atmospheric radiometry. He left JPL to join the faculty in the Department of Electrical Engineering at Pennsylvania State University, University Park, in 1992. His current research activities include ground-based atmospheric radiometry, synthetic aperture interferometric radiometry, continued involvement with the TOPEX/Poseidon mission and related work for the GEOSAT follow-on water vapor radiometer, and millimeter wave propatation studies for the remote sensing of precipitation.

Dr. Ruf is an Associate Editor for *Radio Science*. He is a member of the AGU and Commission F of URSI. He is a past Associate Editor of the University Profiles column in the IEEE Geoscience and Remote Sensing Society Newsletter. He presently serves on the technical steering committee for the 1996 IEEE/URSI International Geoscience and Remote Sensing Symposium in Lincoln, NE and on the technical program committee for the 1996 Specialists Meeting on Microwave Radiometry and Remote Sensing in Boston, MA. He is also presently a member of the IEEE Geoscience and Remote Sensing Society Instrumentation/Future Technologies Committee.

**Rajiv P. Dewan** received the B.S. degree in electrical engineering from Pennsylvania State University, University Park, in May 1993.

He is presently completing the M.S. degree in electrical engineering at Penn State while working full-time in the field of distributed computer system software fault tolerance, availability, and reliability testing at the System/Technology Development Corporation of Herndon, VA.

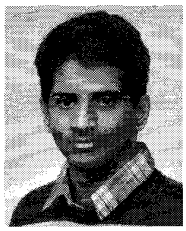

**Bala Subramanaya** (M'96) received the Master of Science degree in electrical engineering from Penn State University, University Park.

He is currently with Hughes STX Corporation at NASA GSFC with the Sensors Development and Characterization Branch. He is currently working on inflight and laboratory calibration of VIS/NIR/IR Imagers.